Genetic optimization of quantum annealing

Pratibha Raghupati Hegde [1,*] Gianluca Passarelli [2] Annarita Scocco [1] and Procolo Lucignano [1]

[1]*Dipartimento di Fisica "Ettore Pancini," Università di Napoli Federico II, 80126 Napoli, Italy*
[2]*CNR-SPIN, c/o Complesso Universitario di Monte S. Angelo, via Cinthia, 80126 Napoli, Italy*

The study of optimal control of quantum annealing by modulating the pace of evolution and by introducing a counterdiabatic potential has gained significant attention in recent times. In this work, we present a numerical approach based on genetic algorithms to improve the performance of quantum annealing, which evades the Landau-Zener transitions to navigate to the ground state of the final Hamiltonian with high probability. We optimize the annealing schedules starting from the polynomial ansatz by treating their coefficients as chromosomes of the genetic algorithm. We also explore shortcuts to adiabaticity by computing a practically feasible k-local optimal driving operator, showing that even for $k = 1$ we achieve substantial improvement of the fidelity over the standard annealing solution. With these genetically optimized annealing schedules and/or optimal driving operators, we are able to perform quantum annealing in relatively short timescales and with higher fidelity compared to traditional approaches.

I. INTRODUCTION

Small spectral gaps are a bottleneck of adiabatic quantum computation and quantum annealing [1–4]. In these paradigms of quantum computation, the goal is to read the ground state of a target Hamiltonian H_z, encoding an NP-complete or NP-hard problem [5]. Starting from the (easy to prepare) ground state $|\psi(0)\rangle$ of a transverse field Hamiltonian $H_x = -\Gamma \sum_{i=1}^{n} \sigma_i^x$, where n is the number of qubits and Γ is the strength of the transverse field, the system is evolved with the time-dependent Hamiltonian $H_0(t) = A(t)H_x + B(t)H_z$. The annealing schedule is given by the pair $\{A(t), B(t)\}$, satisfying $A(0) \gg B(0)$ and $0 = A(T) \ll B(T)$, where T is the annealing time. At $t = T$, the system is found in the target ground state with a high probability, provided T is longer than the inverse square of the smallest gap between the ground state and the first excited state [6]. During the dynamics the system may cross a quantum phase transition [7]; correspondingly, the gap takes its minimum value $\Delta = \min_t[E_1(t) - E_0(t)]$, which results in long annealing times to satisfy the adiabatic condition, thus making the algorithm ineffective.

If the annealing time T is shorter than that predicted by the adiabatic theorem, the fidelity of the final solution is compromised; if T is longer, the system suffers decoherence. Therefore, the goal here is to modify the annealing dynamics in order to achieve high fidelities, even breaking the adiabatic criterion, before decoherence sets in. This can be achieved by taking advantage of different improved schemes. We mention optimal control theory [8], which is limited, in principle, only by the quantum speed limit [9,10]; shortcuts to adiabaticity (STAs) [11–23]; and modulating in a controlled way the annealing schedules [24–27].

A possible STA consists in adopting counterdiabatic (CD) driving [11–18]. In transitionless or CD driving, a time-dependent potential $H_{CD}(t)$ is added to the unperturbed Hamiltonian $H_0(t)$ so that diabatic Landau-Zener transitions are completely suppressed at all times and for all choices of the annealing time T. The total Hamiltonian reads $H(t) = H_0(t) + H_{CD}(t)$. The CD operator satisfies the constraint $H_{CD}(0) = H_{CD}(T) = 0$ and does not modify the starting and target Hamiltonians. Computing the exact CD potential requires knowledge of the (generally unknown) instantaneous spectrum of the Hamiltonian $H_0(t)$. Moreover, the resulting operator is highly nonlocal, hardly implementable on actual quantum machines, and generally unbounded in the thermodynamic limit [28].

Recently, much effort has been put forth to build approximate CD potentials. In some very simple cases, such as the Ising model with longitudinal and transverse fields, linear combinations of local operators provide good approximations of the CD potential, e.g., $H_{CD}(t) \approx \sum_k \alpha_k(t)O_k$. The operators O_k are generally Hermitian products of a small number of Pauli operators. The coefficients $\alpha_k(t)$ can be determined by variational optimization [29,30]. For more complicated many-body Hamiltonians, other choices for operators O_k involve nested commutators between $H_0(t)$ and its time derivative [31]. However, in the former case, we do not know in advance which and how many local operators are needed to build a good "enough" CD operator. In the latter case, nested commutators can be highly nonlocal, as much as the exact CD potential. Moreover, the number of nested commutators is expected to diverge in the thermodynamic limit when the system undergoes a quantum phase transition [32].

In this paper we derive an alternative route and we focus on the study of optimal annealing schedules $A(t)$ and $B(t)$ and an optimal driving (OD) potential $H_{OD}(t)$ that are variationally improved to achieve the maximum fidelity at the final time

*pratibharaghupati.hegde@unina.it

T. The search for variational minima is approached using computational intelligence tools [26]; in particular, we adopt a genetic algorithm, i.e., an evolutionary strategy inspired by the Darwinian theory of the survival of the fittest [33]. We consider time schedules that are polynomial functions of time and we consider local operators for the OD. In our approach, the coefficients of the polynomials and the OD operator are represented as a real-valued chromosome. Each chromosome is characterized by a fitness value. At each generation, chromosomes will mate and randomly mutate. Only the fittest individuals will survive to the next generation. We show that a simple choice of the fitness function can lead to optimized annealing schedules as well as to OD potentials that largely improve the fidelity of the target quantum ground state of H_z, compared to the bare case. We discuss the adiabatic quantum computation of a prototypical system, the ferromagnetic p-spin model, an exactly solvable model with a nontrivial phase diagram, which encodes a Grover-like search [27,34] for large and odd p.

This paper is organized as follows. In Sec. II we describe the ferromagnetic p-spin model. In Sec. III we introduce the genetic algorithms and the construction of chromosomes for the problems of optimization of annealing schedules and OD potentials. We also define fitness functions for single-objective genetic algorithms (SOGAs) and multiobjective genetic algorithms (MOGAs). In Sec. IV we present the results obtained by optimizing the annealing schedules and OD potentials individually and together using genetic algorithms. In Sec. V we discuss the possibility of extending our techniques to the quantum annealing of random Ising models. We summarize in Sec. VI.

II. DEFINITION OF THE PROBLEM

In this paper we consider the fully connected ferromagnetic p-spin model [35,36] as a case study. The Hamiltonian of this model is

$$H_z = -Jn \left(\frac{1}{n} \sum_{i=1}^{n} \sigma_i^z \right)^p, \tag{1}$$

with $J > 0$ and $p \geqslant 2$. For odd p, its ground state is ferromagnetic with all qubits in the state $|0\rangle$. For even p, the ground-state manifold is two dimensional ($|00\cdots0\rangle$ and $|11\cdots1\rangle$) due to the Z_2 symmetry. If we study the quantum annealing with the time-dependent Hamiltonian $H_0(t)$ using as a target Hamiltonian H_z defined in Eq. (1), we observe a dynamical quantum phase transition separating a paramagnetic phase (at short times) from a ferromagnetic phase (at long times). For $p = 2$, the quantum phase transition is of second order, while for $p \geqslant 3$ it is of first order. The latter is the hardest case for quantum annealing, as the minimal gap Δ closes exponentially as a function of n [37]. This feature motivates the broad interest in this system as a toy model of NP-hard problems [32,38–47].

The model Hamiltonian is permutationally invariant and commutes with the total spin operator S^2 at all times. The starting and the target state belong to the subspace with maximum spin $S = n/2$ and the dynamics will occur within the same (maximum spin) subspace. Therefore, we can work in this ($N = n + 1$)-dimensional sector. In the following, we will

consider J as the unit of energy. Times are expressed in units of J^{-1} ($\hbar = 1$ here and in the following).

We perform adiabatic evolutions of the system described by the p-spin model assisted by genetic algorithms. We aim at improving the final-state fidelity of the system by following three strategies: (a) optimizing annealing schedules, (b) optimizing local OD with the traditional linear annealing schedules, and (c) optimizing both annealing schedules and the local OD operator. These strategies are explained in detail later in the paper (see Sec. III). Further, we choose an annealing time sufficiently shorter than the timescale T_{ad} predicted by the adiabatic theorem, i.e.,

$$T_{ad} = \max_{\lambda \in [0,1]} \frac{|\langle E_0(\lambda)|\partial_\lambda H(\lambda)|E_1(\lambda)\rangle|}{|E_1(\lambda) - E_0(\lambda)|^2}, \quad \lambda = t/T. \tag{2}$$

III. METHODS: GENETIC ALGORITHMS

We use a class of evolutionary algorithms known as genetic algorithms to find optimized annealing schedules for adiabatic evolutions. In addition, we also manage to demonstrate the efficiency of genetic algorithms in the paradigm of shortcuts to adiabaticity by finding optimized local OD operators.

Genetic algorithms are inspired by Darwin's theory of evolution. These algorithms offer solutions to optimization problems conditioned by a single objective or multiple objectives [46,48–50]. In both cases, the possible solutions to the problem are encoded as a string of real numbers called chromosomes. The construction of a chromosome depends on the optimization problem. In this article, broadly speaking, we address three optimization problems, all of which aid the performance of adiabatic evolution, i.e., finding the system in a ground state of the problem Hamiltonian H_z with maximum probability at the end of the evolution. The three problems are as follows.

A. Optimization of annealing schedules

Here we try to optimize the performance of quantum annealing by optimizing its annealing schedules $A(t)$ and $B(t)$ [24–26]. First, we express the annealing schedules as dimensionless time functions of $s = t/T$ throughout this paper. We consider polynomial expansions of $A(s)$ and $B(s)$ as candidates for the possible annealing time schedules, i.e., $A(s, \alpha) = \sum_{i=1}^{k_a+1} \alpha_i s^i$ and $B(s, \beta) = \sum_{j=1}^{k_b+1} \beta_j s^j$. Moreover, these time-dependent functions have to satisfy the boundary conditions $A(0) = 1$ and $A(1) = 0$, and $B(0) = 0$ and $B(1) = 1$, respectively, and therefore can expressed as

$$A(s, \alpha) = 1 + \sum_{i=1}^{k_a} \alpha_i s^i + \left(-1 - \sum_{i=1}^{k_a} \alpha_i \right) s^{k_a+1},$$

$$B(s, \beta) = \sum_{j=1}^{k_b} \beta_j s^j + \left(1 - \sum_{j=1}^{k_b} \beta_j \right) s^{k_b+1}. \tag{3}$$

We optimize the coefficients of these polynomial expansions as chromosomes of the genetic algorithm and the structure of the chromosome for this problem is

$$D_1 = [\alpha_1, \alpha_2, \dots, \alpha_{k_a}, \beta_1, \beta_2, \dots, \beta_{k_b}]. \tag{4}$$

The length of the chromosome is $k_a + k_b$.

B. Optimization of the local OD operator

In this section we adopt the strategy of shortcuts to adiabaticity to optimize the performance of quantum annealing [28–32]. Keeping the annealing schedules fixed and as linear functions, i.e., $A(s) = 1 - s$ and $B(s) = s$, we optimize an OD operator which successfully avoids Landau-Zener transitions, resulting in a better fidelity of the state of the system with the exact ground state at $t = T$. We assume that the OD operator $H_{OD}(s)$ can be expanded as the sum of local spin operators,

$$H_{OD}(s, \gamma) = C(s) \sum_{i=1}^{d} \gamma_i O_i, \qquad (5)$$

where O_i are the total spins in the x, y, and z directions, i.e., S_x, S_y, and S_z, and their products. In particular, we consider only single local operators and cumulatively add the set of all possible two-spin operators and the set of all three-spin operators. These local operators can be explicitly written as

$$H_{OD}(s, \gamma)_{d=3} = C(s) \sum_{i=1}^{3} \gamma_i S_i,$$

$$H_{OD}(s, \gamma)_{d=9} = H_{OD}(s)_{d=3} + C(s) \sum_{i,j=1}^{3} \gamma_{i,j} S_i S_j,$$

$$H_{OD}(s, \gamma)_{d=21} = H_{OD}(s)_{d=9} + C(s) \sum_{i,j,k=1}^{3} \gamma_{i,j,k} S_i S_j S_k. \quad (6)$$

The chromosome of the genetic genetic algorithm for this problem is the set of coefficients of the local operators

$$D_2 = [\gamma_1, \ldots, \gamma_3, \gamma_{11}, \gamma_{12}, \ldots, \gamma_{33}, \gamma_{111}, \gamma_{112}, \ldots, \gamma_{333}] \qquad (7)$$

whose length is equal to the number of local operators d. In this work we are able to achieve remarkable results by optimizing the local OD operator with only single-spin operators, i.e., $H_{OD}(s, \gamma)_{d=3} = C(s) \sum_{i=1}^{3} \gamma_i S_i$, and therefore we discuss and demonstrate our results for the case with $d = 3$. The higher terms of two-spin and three-spin operators are omitted since they do not produce any significant improvements. The time schedule $C(s)$ is fixed in this approach and is given by $C(s) = A(s)B(s) = (1 - s)s$. The function $C(s)$ controls the pace of evolution dictated by the OD operator $H_{OD}(s)$.

C. Optimization of the time schedules and the local OD

Here we optimize the annealing schedules $A(s)$ and $B(s)$ and the local OD operator altogether [24,25]. The time schedule $C(s)$ is optimized by absorbing it as the coefficients of the local OD operators, i.e., $H_{OD}(s) = \sum_{i=1}^{d} C_i(s) O_i$. We consider each $C_i(s)$ to be a polynomial of order $k_c + 1$, which satisfies the boundary conditions $C_i(0) = 0$ and $C_i(1) = 0$. Therefore, the OD operator can be explicitly written as

$$H_{OD}(s, \epsilon) = \sum_{i=1}^{d} \left[\sum_{j=1}^{k_c} \epsilon_{ji} s^j + \left(-\sum_{j=1}^{k_c} \epsilon_{ji} \right) s^{k_c+1} \right] O_i. \qquad (8)$$

We optimize the free parameters ϵ_{ji}, in addition to the free parameters α_i and β_i in Eq. (4). The time-dependent Hamiltonian of the system is given by

$$H(s) = A(s, \alpha)H_x + B(s, \beta)H_z + H_{OD}(s, \epsilon), \qquad (9)$$

where

$$\alpha = \{\alpha_1, \ldots, \alpha_{k_a}\},$$
$$\beta = \{\beta_1, \ldots, \beta_{k_b}\},$$
$$\epsilon = \{\epsilon_{11}, \ldots, \epsilon_{k_c d}\}.$$

Therefore, the chromosome for this optimization problem can be expressed as

$$D_3 = [\alpha_1, \ldots, \alpha_{k_a}, \beta_1, \ldots, \beta_{k_b}, \epsilon_{11}, \ldots, \epsilon_{k_c 1}, \ldots, \epsilon_{k_c d}]. \qquad (10)$$

The length of the chromosome in this case is $k_a + k_b + (d \times k_c)$. Here again we are able to obtain high fidelity of the state of the system by considering only single-spin operators in the expansion of the local OD operator. Therefore, we stick to the case of $d = 3$.

The key aspect of genetic algorithms is the definition of the fitness function. It is a function which takes each chromosome as a variable and gives it a fitness value according to the quality of the solution generated by the given chromosome. In the course of a genetic algorithm, we intend to either maximize or minimize this fitness function. Depending on the number of conditions the chromosomes have to satisfy, the genetic algorithms are characterized by fitness functions which are single objective or multiobjective. In the rest of this section, we describe the fitness function and the workflow of SOGAs and MOGAs.

D. Single-objective genetic algorithms

Single-objective genetic algorithms follow the workflow of a standard genetic algorithm. We define the fitness of each chromosome as the fidelity, which is the ground-state probability at $t = T$, i.e.,

$$f_{SO} \equiv P_{gs}(T) = |\langle E_0(T)|U(T)|\psi(0)\rangle|^2, \qquad (11)$$

where $U(t, 0) = \mathcal{T}_+ \exp\{-i \int_0^t [H(t')]dt'\}$ is the time-evolution operator and $\mathcal{T}_+$ is the time ordering.[1] An alternative fitness function would be to use the negative of the mean energy at the final time T, i.e., $-\langle \psi(0)|U^\dagger(T, 0)H_z U(T, 0)|\psi(0)\rangle$. This choice does not require the knowledge of any spectral property of the Hamiltonian. The fittest individuals, maximizing f_{SO}, are those with higher fidelities and are likely to survive along generations. At the end of the genetic optimization, we will obtain a chromosome defined according to the problem. However, all three problems considered here aim at giving a higher fidelity.

We initialize a starting population of N_{pop} individuals, whose genes are randomly extracted in the interval $[g_{min}, g_{max}]$. Then we repeatedly apply the three genetic operators (mutation, crossover, and selection [53]) until a convergent solution is achieved. The genetic algorithm is implemented using the DEAP package [50]. Here we briefly describe the genetic operators adopted, also sketched in Fig. 1.

---

[1]The time evolution is computed with the QUTIP toolbox [51,52].
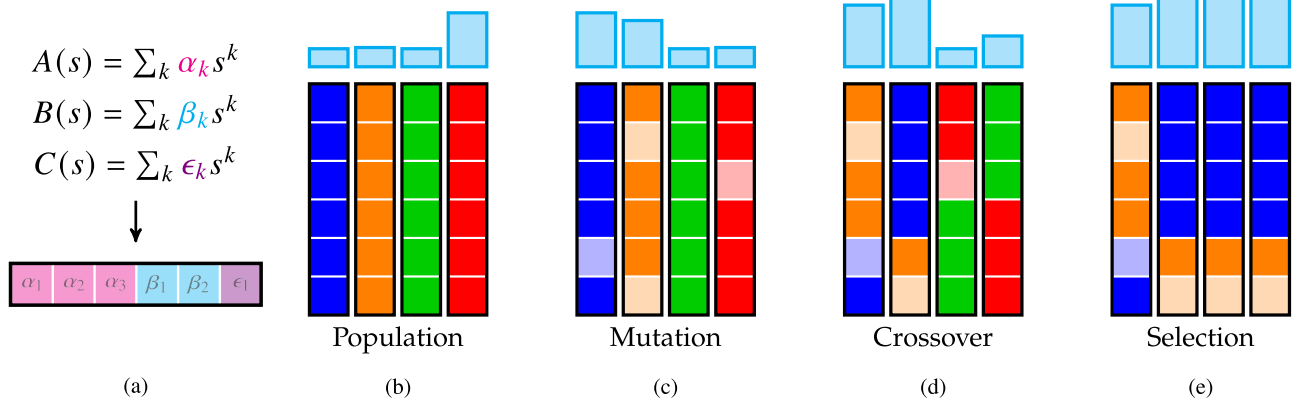
FIG. 1. Cartoon of our genetic algorithm. (a) The free parameters of the annealing schedules are stored in a chromosome. (b) We first randomly generate N_{pop} individuals. (c) Then random gene mutation occurs in each individual. (d) Then we apply two individual crossovers. (e) We select the fittest individuals and start again from (c) until convergence. The azure bars identify the fitness values: the larger the better.

(i) Gaussian mutation. Among the population of individuals, random individuals are selected with a probability P_m for mutation. Each gene is independently mutated with a probability P_{ind}, by adding a normal variable, extracted from a Gaussian with mean value $\mu = 0$ and variance $\sigma^2 = 1$ [see Fig. 1(c)]. The mutation probability of each gene, i.e., the product $P_m P_{ind}$, should be neither too high nor too low (a quantitative description is given in Appendix A). In the former case, the genetic algorithm will turn into a random search. In the latter case, the algorithm would be nonergodic. These random mutations increase variability in the population and reduce the probability of being trapped in local minima.

(ii) Two-point crossover. After the mutation process, we randomly select two parents from the chromosome population. Two random integers are randomly extracted from the interval $[0, L-1]$, where L is the length of the chromosome, which is the number of free parameters to be optimized using a genetic algorithm and is problem specific. Two children are produced by mixing alternating parts of the two parents, obtained by cutting the chromosomes at the two extracted indices [see Fig. 1(d)]. Note that the exchange of the fragments is only symbolic in Fig. 1(d) and represents a one-point crossover for the sake of visual clarity. In our experiments, we resort to a two-point crossover operator, which yields the fastest convergence in this case. The whole process occurs with a probability P_c. Low P_c ensures slow but accurate convergence to the optimal solution. On the other hand, high P_c ensures quick convergence but can lead to suboptimal solutions. Hence, P_c has to be carefully tuned to find a compromise between speed of convergence and accuracy of the solution.

(iii) Selection by tournament. After mutation and crossover, a new population is produced. N_T competitors are selected from the population and their fitness is compared [see Fig. 1(e)]. Only the fittest individual survives to the next generation. This tournament is repeated until we obtain a new set of N_{pop} individuals.

E. Multiobjective genetic algorithms

While SOGAs aim at maximizing the ground-state probability at the final time T, they sometime lead to practically infeasible solutions during the time of evolution. For example,

some of the solutions returned by the algorithm can have energy-level crossings between the ground state and the first excited state. In an attempt to avoid these solutions produced by SOGAs, we add another objective to the fitness function. Other than maximizing the fidelity at $t = T$, we choose to maximize it together with the area under the curve of the instantaneous ground-state probabilities of the system computed at N_t time intervals. The latter ensures that the ground-state occupation is maximum at all the intermediate times, in the spirit of counterdiabatic dynamics. The ground-state probability at time t is given by $P_{gs}(t) = |\langle E_0(t)|U(t)|\psi(0)\rangle|^2$. The fitness of a chromosome in MOGAs is defined as

$$f_{MO} \equiv \left\{ \frac{1}{T} \int_0^T P_{gs}(t) dt, P_{gs}(T) \right\}. \qquad (12)$$

We stress here the fact that this is not the same as imposing local adiabaticity as by Roland and Cerf [27]. Multiobjective genetic algorithms deviate from the standard genetic algorithms. In particular, they work using the strategy of a nondominated sorting genetic algorithm (NSGA-II) [49,54]. NSGA-II uses an elitist method of evolutionary algorithms. The parent and offspring generations are grouped together and are ranked into fronts based on nondominated sorting. The population of the following generation is filled with the best fronts until N_{pop} is reached. In the case in which only some chromosomes have to be selected from a front in the process, the most diverse solutions are chosen based on the crowding distance. Given the new population, by the above nondominated sorting process, the chromosomes undergo selection (a binary tournament selected based on both rank and crowding distance), mutation, and crossover processes. At the end of N_{gen} generations, the Pareto optimal front with the best ranking is obtained. The details of selecting the chromosome from the Pareto optimal front is given in Appendix B.

IV. RESULTS

In this section we present the results obtained by performing adiabatic quantum computation of the ferromagnetic p-spin model assisted by genetic algorithms. In particular, we concentrate on a system with 15 spins and $p = 3$ to demonstrate our results. The adiabatic timescale of Eq. (2)

for this system is $T_{ad} \approx 30$. We choose the annealing time $T = T_{ad}/10 \approx 3$ in order to be far from adiabaticity. Throughout the time evolution, we store the data of energy gaps between the ground state and the first excited state, time schedule function values, and ground-state probabilities. We initiate the genetic algorithm with a population of $N_{pop} = 20$ individuals and run it for a large enough number of generations until the algorithm gives convergent values. When implementing genetic algorithms, it is advisable to perform initial experimentation to optimize the hyperparameters involved in mutation, crossover, and selection processes. The details of this procedure are given in Appendix A. We consider the optimal hyperparameters to repeatedly perform genetic algorithms and to analyze the results obtained from their solutions. With the optimized annealing schedules and an optimal driving operator, the Schrödinger equation is solved in the time domain $[0, T]$ and sampled at 100 evenly spaced points in this interval. The system is initialized in the ground state of H_x. When we optimize the annealing schedules, we evolve the Schrödinger equation with the Hamiltonian in Eq. (9), but without the optimal driving term $H_{OD}(s, \epsilon)$. In the case of optimal driving optimization, we evolve the Schrödinger equation with the Hamiltonian in Eq. (9). The ground-state probability of the system is computed along the genetically optimized path of quantum annealing. The Schrödinger equation evolution is simulated using the QUTIP library [51,52]. Further, we repeat the genetic algorithms 50 times and compute the corresponding results pertaining to the dynamics of the system. Hereafter, we present the results obtained by using the three strategies assisted by a SOGA. We discuss the cases where MOGAs can be chosen over SOGAs in order to obtain meaningful results. Further, we test our methods in systems with a varying number of spins.

A. Optimization of annealing schedules $A(s)$ and $B(s)$

As described in Sec. III, we optimize the annealing schedules by encoding the coefficients of the polynomials in Eq. (3) as chromosomes D_1 in Eq. (4). With the optimal annealing schedules given by the genetic algorithms, we simulate the adiabatic quantum computation. We focus on the cases when $k_a = 2$ and $k_b = 2$ and hence the length of the chromosome is 4. We have run the algorithm for 5000 generations.

The summary of the results from optimizing the annealing schedules using the SOGA is provided in Fig. 2. In Fig. 2(a) we show that the optimized path increases the minimum gap between the ground state and the first excited state only slightly: The energy scales remain within practical limits. Meanwhile, in Fig. 2(b) the ground-state probabilities remain higher throughout the evolution and around the final time there is a slight drop in the fidelity. This could possibly be overcome by using a MOGA by imposing a condition on the fitness function that the derivative of the ground-state probability evolution curve remains smaller. In Fig. 2(c) we show the annealing schedules optimized by the SOGA. We see that both schedules $A(s)$ and $B(s)$ increase to a value larger than one and gradually decrease to their respective boundary values, as opposed to the traditionally used monotonic functions [6,46]. We point out that the nature of our optimized time schedules is different from the exact solution of annealing
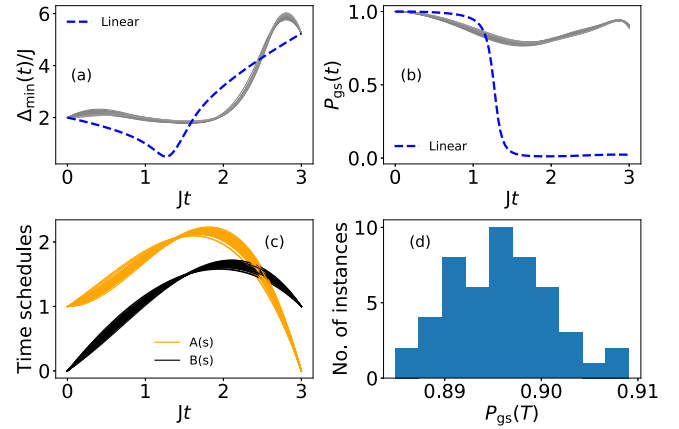

FIG. 2. Summary of the results obtained by using the optimized annealing schedules for solving the p-spin model using SOGAs: (a) instantaneous energy gaps during the dynamics of the adiabatic evolution, (b) instantaneous ground-state probability using the optimized schedules and using a simple linear schedule, (c) annealing schedules $A(s)$ and $B(s)$, and (d) histogram of the fidelities for 50 runs of the algorithm. We investigate the system with 15 spins with both annealing schedules $A(s)$ and $B(s)$ expanded up to a degree of 3. In other words, $k_a = k_b = 2$.

schedule function derived, for example, in Ref. [27]. This is due to the fact that we do not impose the local adiabaticity at all points of time, but only at the final time. Figure 2(d) shows the histogram of fidelities for 50 runs of the algorithm. Fidelities are distributed in a small window with the median value of the distribution approximately equal to 0.895, which is about two orders of magnitude higher with respect to the linear schedule.

To conclude this section, we study the genetic optimization of annealing schedules for varying system sizes. In Fig. 3
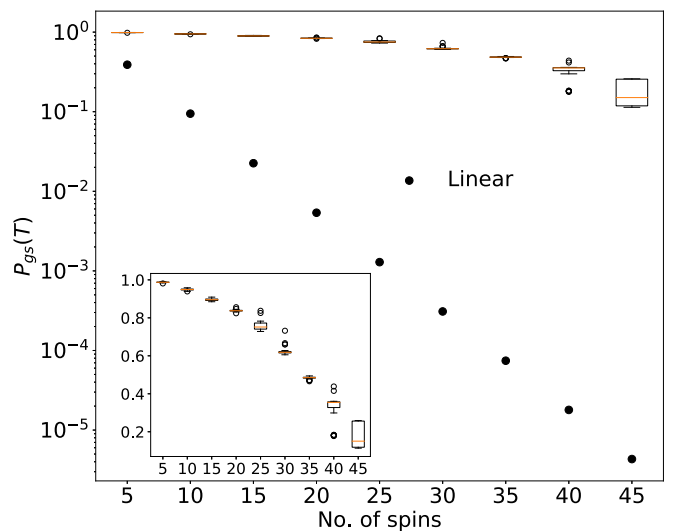

FIG. 3. Box plot of fidelities of the states of systems with different sizes. Each box represents the first quartile and the third quartile and the red (gray) dashed line represents the median of the data for 50 runs of the SOGA which optimizes the annealing schedules $A(s)$ and $B(s)$, each of which is expanded up to a third-degree polynomial.
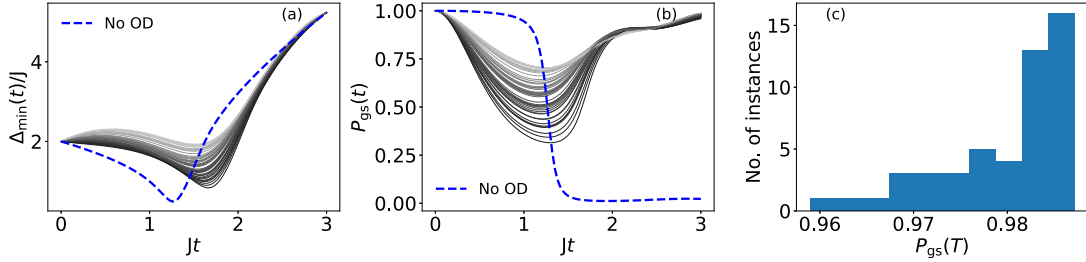
FIG. 4. Results obtained by optimizing the time-independent part of the local OD operator for the ferromagnetic p-spin model with 15 spins and $p = 3$. The OD operator chosen is $H_{OD}(s, \gamma)_{d=3}$. The plots depict the data for 50 runs of the SOGA and the corresponding results obtained by adiabatic quantum computation. (a) Instantaneous energy gaps between the ground state and the first excited state. (b) Instantaneous ground-state probabilities. (c) Histogram of the fidelities for 50 instances.

we set the chromosome length equal to 4 and we run the genetic algorithms for 5000 generations for system sizes up to 45 spins. We plot the fidelities of the adiabatic evolution as a box plot, where each box represents the interval between the first and third quartiles and the red (gray) dashed line is the median fidelity over 50 repetitions. The solutions by the genetic algorithms decrease for larger system sizes. However, the performance is strikingly better than the corresponding results using linear annealing schedules, by several orders of magnitude.

B. Optimization of OD

Here we optimize the local OD operators alone, fixing linear annealing schedules as described in Sec. III. The chromosome is D_2 in Eq. (7). We focus on optimizing the local operators with only single-spin operators $H_{OD}(s, \gamma)_{d=3}$ from Eq. (6) and show that by optimizing only three parameters, we obtain good fidelities. The higher number of local terms leads to many trivial solutions of simply increasing the energy scale of the system beyond practical capabilities due to the large solution space, at the same time being computationally expensive.

A summary of the results obtained by genetic optimization of $H_{OD}(s, \gamma)_{d=3}$ is shown in Fig. 4. In Fig. 4(a) we show the energy gaps between the ground state and the first excited state. The minimum energy gap is slightly higher than the original system driven with no OD potentials. In Fig. 4(b) we show the corresponding results of the evolution of ground-state probabilities. Even though the ground-state probabilities are comparatively lower during the evolution, the fidelities are high at the final time. The probabilities can be controlled to be higher also during the evolution using a MOGA. The results are not very diverse due to the small chromosome size and yet this set of solutions is feasible. Finally, in Fig. 4 we show the distribution of fidelities for 50 solutions of the SOGA. All the solutions show very high fidelity with a median value approximately equal to 0.98. We analyze the data of optimized chromosomes to understand the contribution of each of the local operator terms in the expansion of the optimized local OD operator. The contribution of S_y is larger for all the cases considered, which is expected since the term S_y is the starting point for many known expansions of the OD operator [29–32].

We verify the robustness of the genetic optimization approach in OD driving for larger system sizes. In Fig. 5 we compare the fidelities of states of the systems up to 45 spins. The fidelities are very high despite increasing the number

of spins by optimizing only single-spin operators (i.e., $d = 3$). Nevertheless, when we increase the size of the system, some of the solutions given by the genetic algorithms lead to energy-level crossings between the ground state and the first excited state. The corresponding ground-state probabilities fall to very low values in these points and regain better values towards the end of the evolution. However, this is an unphysical scenario. We resort to a MOGA in this case, which makes sure the ground-state probabilities are higher throughout the evolution by avoiding the situations of energy crossings. An example of improvement of the results using a MOGA for a system with 40 spins is demonstrated in Appendix B.

C. Optimization of time schedules and local OD

Here we optimize the free parameters of the time schedules $A(s, \alpha)$, $B(s, \beta)$, and $C(s, \epsilon)$ all together as a chromosome D_3 in Eq. (10). We choose $k_a = 2$, $k_b = 2$, and the number of local operators $d = 3$, each accompanied by a time schedule $C_i(s, \epsilon)$ as described in Eq. (8) with $k_c = 3$. It is sufficient to run the algorithm up to 1000 generations in this case in order to obtain convergent results.

Figure 6 shows a summary of the results obtained by optimizing all the time schedules in the realm of shortcuts to
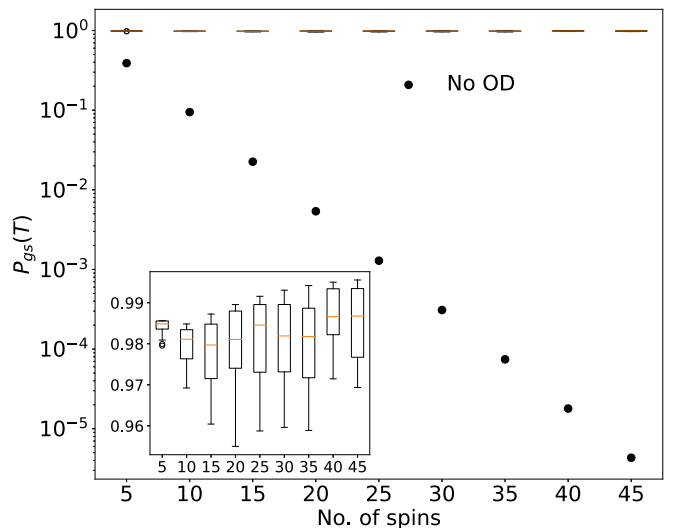

FIG. 5. Box plot of fidelities of the states of systems with different sizes. Each box represents the data for 50 runs of the SOGA iterated for 1000 generations, which optimizes the time-independent part of the OD operator with $d = 3$.
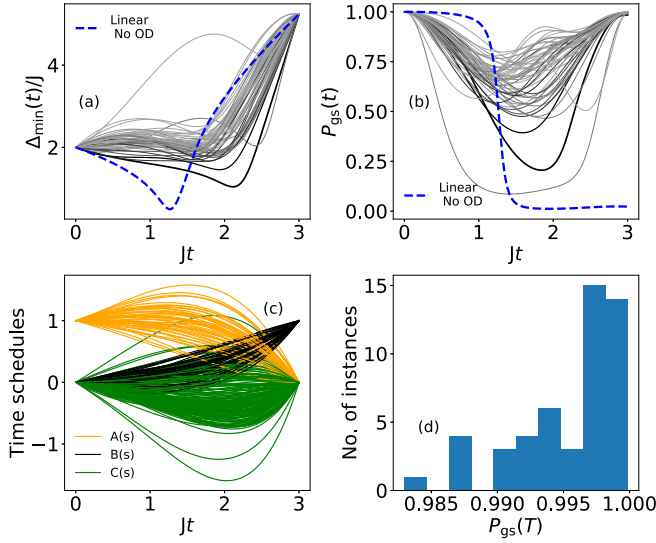
FIG. 6. Results obtained by optimizing the annealing schedules $A(s)$ and $B(s)$ and time-dependent local OD operator for the ferromagnetic p-spin model with 15 spins and $p = 3$. The OD operator chosen is $H_{\text{OD}}(s, \gamma)_{d=3}$, $k_a = k_b = 2$, and $k_c = 3$. The plots depict the data for 50 runs of the SOGA and the corresponding results obtained by adiabatic evolution. (a) Instantaneous energy gaps between the ground state and the first excited state. (b) Instantaneous ground-state probabilities. (c) Time schedule functions $A(s)$, $B(s)$, and $C(s)$. (d) Histogram of the fidelities for 50 instances.

adiabaticity. In Fig. 6(a) we show the minimum energy gaps. In this case, the solutions are quite diverse because of the larger search space. The same is reflected in the evolution of ground-state probabilities in Fig. 6(b). In Fig. 6(c) we show the optimized annealing schedules. While some of the solutions show the same increase and decrease patterns seen in the previous case, some others are monotonic between the boundary values. The schedules $C(s)$ plotted in green are composed of the three time functions $\{C_1(s), C_2(s), C_3(s)\}$ of each of the local operators in the expansion of the OD potential. We show the distribution of fidelities in the solutions given by the genetic algorithm in Fig. 6(d). The fidelities are exceptionally higher with a median value approximately equal to 0.997.

In Fig. 7 we compare the fidelities of adiabatic quantum computation assisted by genetic algorithms for varying system sizes. Here we have set the chromosome length to be 13 and we run the algorithm for 1000 generations for all the cases. The performance of genetic optimization is consistently higher even for larger system sizes.

V. GENERALIZATION TO RANDOM ISING MODELS

In order to test the feasibility of our method in a more general framework, we additionally study the performance of the genetic optimization for a random Ising model. We consider a system of $n = 5$ qubits arranged in the graph shown in Fig. 8, described by the Hamiltonian

$$H_z = H_{\text{I}} = \tfrac{1}{2} \sum_{\langle ij \rangle} (\mathbb{1} - J_{ij}\sigma_i^z\sigma_j^z), \tag{13}$$

where the sum acts on qubits connected by the graph bonds and the couplings J_{ij} are random uniform variables in $[-1, 1]$.
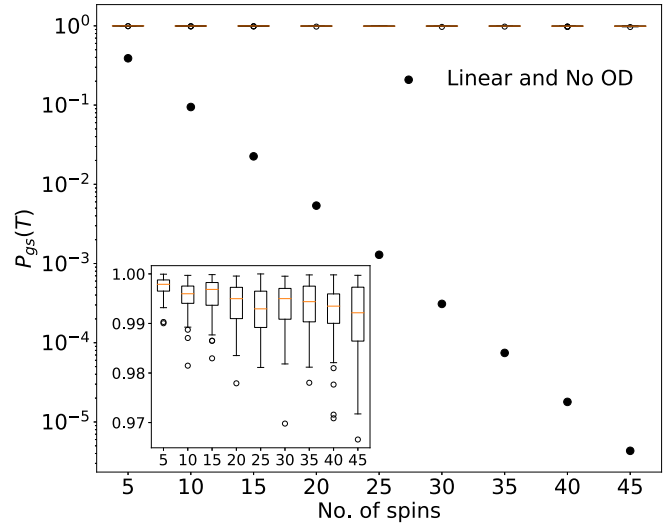

FIG. 7. Box plot of fidelities of the states of systems with different sizes. Each box represents the data for 50 runs of the SOGA iterated for 1000 generations, which optimizes the annealing schedules $A(s)$ and $B(s)$ and the scheduling of the local OD operator $[H_{\text{OD}}(s, \gamma)_{d=3}]$, with $k_a = k_b = 2$ and $k_c = 3$.

The idea here is to apply the genetic routine to a family of randomized models to see if some general features of optimized annealing schedules or OD operators can be inferred. This would allow us to significantly speed up computation since it would remove the need to repeat the genetic optimization on an instance-by-instance basis. We generate $N_{\text{inst}} = 50$ random instances and repeat the (stochastic) genetic optimization $N_{\text{rep}} = 30$ times for each instance and for each choice of the parameters of the simulation. In particular, we consider two different annealing times ($T = 5$ and 10). For the optimization of annealing schedules alone, we consider the parameters of the polynomial ansatz, $k_a = k_b = 3$, while for the optimization of the OD operator we consider $k_a = k_b = 2$ and $k_c = 3$. We focus our attention on SOGAs and since the target Hamiltonian is Z_2 symmetric and the ground state is doubly degenerate we resort to the average final energy as the fitness function: $f_{\text{SO}} = \langle H_{\text{I}} \rangle$. We quickly note that the Hamiltonian in Eq. (13) is commonly used to encode MaxCut and MinCut problems [55]. This is why, in the following, we will show data concerning the so-called approximation ratio, i.e., the ratio between the final fitness value and the true
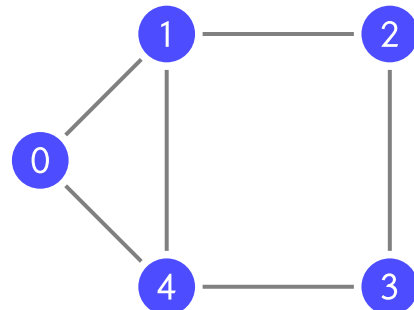

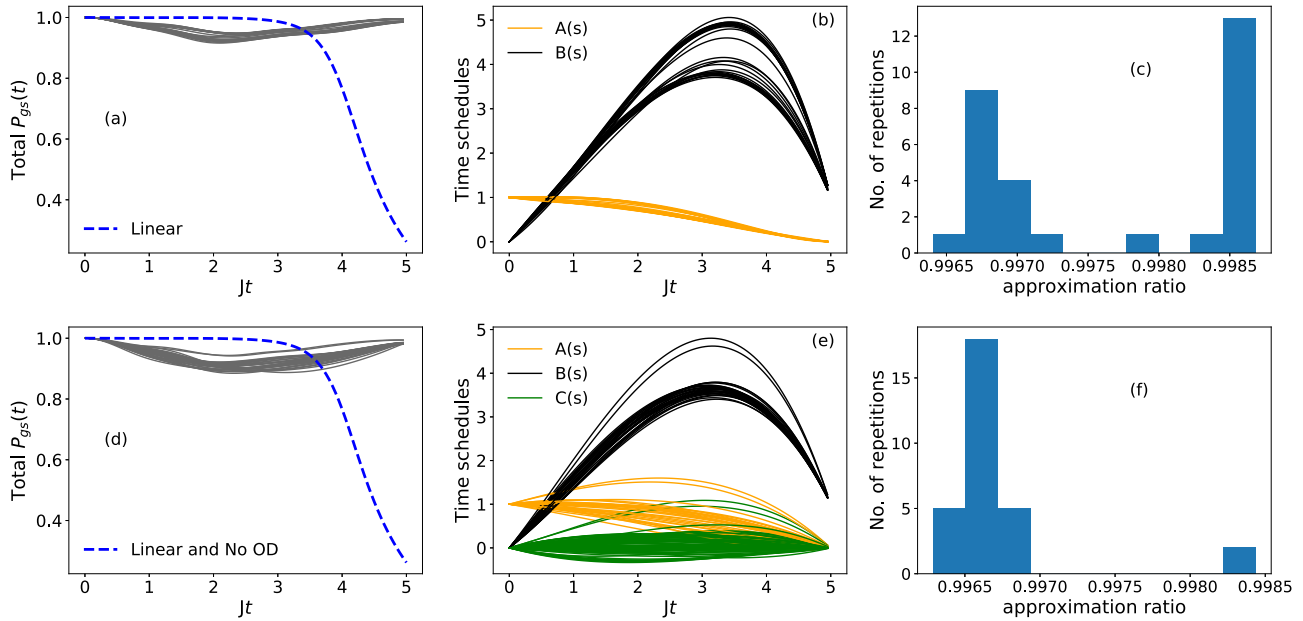FIG. 8. Graph of the Ising model discussed in Sec. V

FIG. 9. Results of genetic optimization of quantum annealing of a random Ising model [Eq. (13)] for a typical random instance. The plot shows the data of 30 genetic optimizations of the considered random instance. (a)–(c) Optimization of annealing schedules alone, with the parameters $k_a = k_b = 3$: (a) instantaneous total probability of obtaining degenerate ground states using optimized polynomial schedules vs using linear schedules, (b) optimized annealing schedules $A(s)$ and $B(s)$, and (c) approximation ratios of 30 genetic optimizations of the given random instance. (d)–(f) Corresponding results obtained by optimizing annealing schedules and the OD operator [$H_{\mathrm{OD}}(s, \gamma)_{d=3}$] together. The parameters considered in this case are $k_a = k_b = 2$ and $k_c = 3$.

ground-state energy, which is a commonly used figure of merit in approximate optimization of this kind of problems [55,56].

We show the results for a typical random instance in Fig. 9 by optimizing annealing schedules alone and by optimizing both annealing schedules and OD operator. First, we focus on the optimization of the annealing schedules [see Figs. 9(a)–9(c)]. In all cases analyzed, the annealing schedules are nonmonotonic like for the p-spin model of Sec. II. In addition, since the final typical energy scale is smaller than the starting one, we note that schedule $B(s)$ is always larger than $A(s)$. The energy scales remain comparable to the ones of linear annealing schedules, but the approximation ratio is substantially improved compared with the linear schedules. The results are similar when annealing schedules and OD operators are optimized together [see Figs. 9(d)–9(f)]. In particular, the annealing schedules continue to show nonmonotonic features, and we note that the schedules of the OD operator $C(s)$ is bounded within a smaller range of values. Also, the approximation ratios are significantly higher than the bare case. In Fig. 10 we compare the median approximation ratios (median of $N_{\mathrm{rep}} = 30$ SOGA repetitions) of 50 random instances of the Ising model. It is evident that the genetically optimized quantum annealing protocols show consistently higher approximation ratios than the traditional quantum annealing with linear annealing schedules and without OD.

Even though the preliminary analysis of this problem shows considerably promising results, the question of whether one can find general optimal schedules or OD operator which optimizes any random instance of Ising model remains open. We consider the average time schedules obtained from the data of 50 random instances and investigate if this averaged

schedule optimizes new random instances. In most cases it shows slight improvement when compared to the bare case. However, our analysis is far from being comprehensive in this test case and we reserve the possibility of expanding on
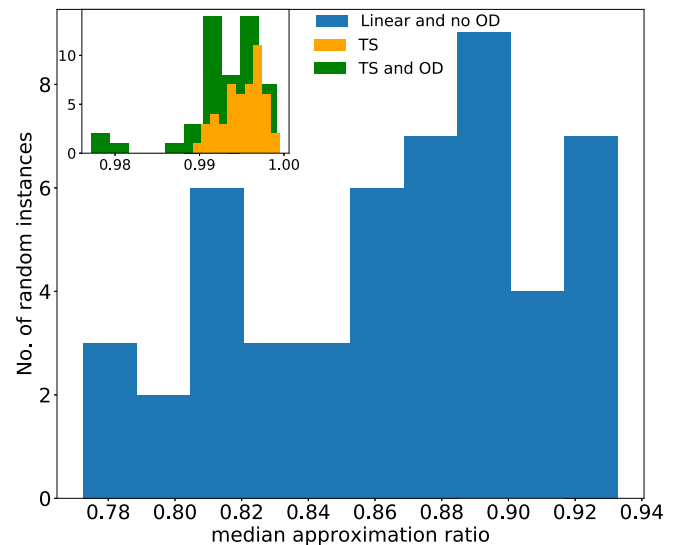

FIG. 10. Median approximation ratio distribution for $N_{\mathrm{inst}} = 50$ random instances over $N_{\mathrm{rep}} = 30$ repetitions of the SOGA for each instance. The histogram shows the approximation ratios of the traditional quantum annealing protocol. The inset shows the corresponding approximation ratios of quantum annealing with optimized time schedules and quantum annealing with optimized annealing schedules and the OD operator.

this aspect in future works together with machine learning techniques.

VI. CONCLUSION

In this paper we used genetic algorithms to optimize the performance of quantum annealing. We demonstrated the efficiency of our method for the ferromagnetic p-spin model with $p = 3$. We optimized the annealing schedules of the standard adiabatic quantum computation protocol using genetic algorithms. We considered the time schedules to be polynomial expansions, whose coefficients were optimized as chromosomes of genetic algorithms. For a system with 15 spins, we were able to achieve a median fidelity approximately equal to 0.895, by optimizing four free parameters of the polynomials.

We used the genetic algorithms in the paradigm of shortcuts to adiabaticity as well. Here we optimized a practically implementable local Hamiltonian composed of only single-spin operators, which when added to the system Hamiltonian can improve the fidelity of the state of the system. In the first step, we fixed the annealing schedules to be linear functions of time and the time schedule of the optimal driving operator to be a quadratic function. By optimizing only the coefficients of single-spin operators, i.e., by optimizing only three free parameters, we were able to achieve a median fidelity approximately equal to 0.98, for a system with 15 spins. As the next step, we optimized the annealing schedules and the time-dependent coefficients of the local operators together. In this case, the time schedules of each of the optimal driving operators were absorbed as their coefficients and were assumed to be polynomial functions of time. By optimizing 13 free parameters of polynomials, we were able to obtain a median fidelity approximately equal to 0.997.

Further, we tested our methodology for varying system sizes. While optimizing annealing schedules alone showed a decrease in the fidelities, optimization of optimal driving showed consistent performance even for larger systems with up to 45 spins by optimizing only local single-spin operators. We also discussed the cases when the single-objective genetic algorithms give unphysical solutions of energy crossings and the possibility of using multiobjective genetic algorithms to tackle this problem.

We tested the technique of SOGAs for a generic case of random Ising models. We generated 50 random instances of Ising models. We separately analyzed the results when only annealing schedules are optimized with chromosome size 6 and as well as in the picture of optimal driving with chromosome size 13. We compared the approximation ratios (the ratio between the energy of the final state and the energy of the true ground state) of the traditional quantum annealing with those of genetically optimized quantum annealing and demonstrated that genetic algorithms are promising tools also in optimizing quantum annealing of random Ising models.

Optimized annealing schedules and local optimal driving operators can enhance the efficiency of quantum annealers in solving optimization problems. To give a practical example, D-Wave quantum annealers allow the experimentalists to control the dynamics globally by submitting a piecewise linear approximation of the annealing schedules. The shape

of this approximation can then be tweaked using our genetic algorithm. Our method is flexible in terms of the choice of the ansatz, the definition of fitness function, and the simulation of time dynamics and can be fine-tuned accordingly to match the experimental platforms and their limitations.

We leave for future work the aim to find general optimal paths of evolution for a class of random Ising models resorting to machine learning techniques, as well as the application of the evolutionary strategies to find shortcuts to adiabaticity for open quantum systems.
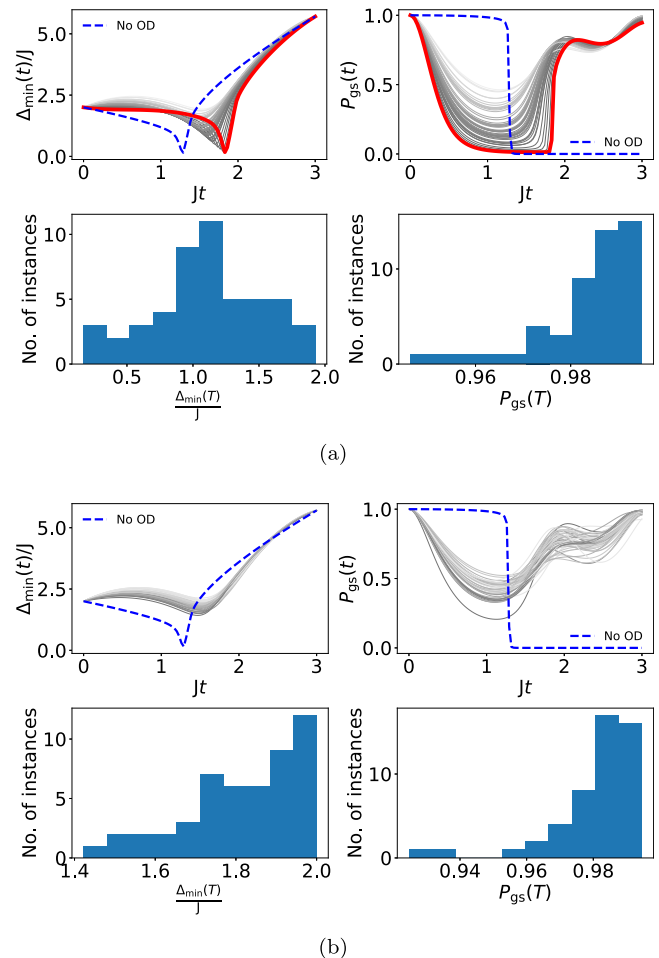
FIG. 11. Results of the optimization of the local OD operator with 3-local operators for a p-spin model with 40 spins and $p = 3$. We compare the performances of (a) SOGAs and (b) MOGAs. The red (dark gray) bold solid lines in the solutions obtained from SOGAs indicate the solutions where there are energy-level crossings. The corresponding results using MOGAs do not show this kind of solution.

APPENDIX A: OPTIMIZING THE HYPERPARAMETERS OF GENETIC ALGORITHMS

Genetic algorithms are characterized by hyperparameters pertaining to the selection, crossover, and mutation processes. To be precise, the individual undergoes the process of mutation with a probability of P_m, wherein the real numbers of the chromosome are altered according to a Gaussian distribution with variance σ^2 and mean μ. Further, each real number (gene) in the chromosome undergoes mutation with the probability P_{ind}. We perform two-point crossover among the parent chromosomes where a string of values is cut and exchanged between the parents to produce two new solutions, this process occurring with a probability of P_c. We choose the tournament selection process where among every N_T individual chromosomes, we choose the best chromosome as the parent for producing offspring. This cycle of generation repeats. In general, for each optimization problem it is advisable to perform an initial experimentation to fix these hyperparameters which give the best solution to the problem [46,48,50]. In particular, for the problem of annealing schedule optimization, we have tuned and chosen the hyperparameters values $N_T = 6$, $P_c = 0.75$, $P_m = 0.35$, $P_{ind} = 0.1$, $\sigma^2 = 0.6$, and $\mu = 0$. For the problem of finding the optimal driving, the best combination of hyperparameters is found to be $N_T = 3$, $P_c = 0.3$, $P_m = 0.9$, $P_{ind} = 0.1$, $\sigma^2 = 1$, and $\mu = 0$. However, in this paper, for the optimization problems chosen, varying the hyperparameters has minimal effect on the overall quality of the solutions. For example, $P_m = 0.9$ gives the best fidelity; however, decreasing P_m leads to searching in a smaller search space, which in turn reduces the number of solutions which simply increase the energy scaling of the system. Meanwhile, by doing so, the fidelity is not affected a great deal.

APPENDIX B: SELECTION OF A CHROMOSOME FROM THE PARETO OPTIMAL FRONT IN A MOGA

The output of a MOGA, which is implemented using NSGA-II, is a set of chromosomes with the best ranking in terms of their domination over the rest of the chromosomes [49,50]. This set of chromosomes is called the Pareto optimal front. At the end of evolution, we choose one of the chromosomes in the Pareto optimal front, which has a good trade-off between the area under the ground-state probability curve and fidelity. In this work we choose the chromosome with the maximum value of $0.4 \times$ (area) $+ 0.6 \times P_{gs}(T)$ and use this solution to perform adiabatic evolution and compute results. As an example, we consider the ferromagnetic p-spin model with 40 spins and optimize a local optimal driving operator (with fixed annealing schedules). We show the difference in the solutions obtained from SOGAs and MOGAs in Fig. 11. In the MOGA, with the imposition of a large area under the curve of ground-state probabilities, the genetic algorithm converges to solutions where there are no energy crossings. The same can be seen in the plots of $\Delta_{min}(t)$ and the histogram of $\Delta_{min}(T)$. The median fidelity using the results of the SOGA is approximately equal to 0.983, whereas with the MOGA, the median fidelity is approximately equal to 0.981.

[1] T. Kadowaki and H. Nishimori, Quantum annealing in the transverse Ising model, Phys. Rev. E **58**, 5355 (1998).

[2] G. E. Santoro, R. Martoňák, E. Tosatti, and R. Car, Theory of quantum annealing of an Ising spin glass, Science **295**, 2427 (2002).

[3] T. Jörg, F. Krzakala, J. Kurchan, A. C. Maggs, and J. Pujos, Energy gaps in quantum first-order mean-field–like transitions: The problems that quantum annealing cannot solve, Europhys. Lett. **89**, 40004 (2010).

[4] S. Knysh, Zero-temperature quantum annealing bottlenecks in the spin-glass phase, Nat. Commun. **7**, 12370 (2016).

[5] A. Lucas, Ising formulations of many NP problems, Front. Phys. **2**, 5 (2014).

[6] M. S. Sarandy, L.-A. Wu, and D. A. Lidar, Consistency of the adiabatic theorem, Quantum Inf. Process. **3**, 331 (2004).

[7] S. Sachdev, *Quantum Phase Transitions*, 2nd ed. (Cambridge University Press, Cambridge, 2011).

[8] S. J. Glaser, U. Boscain, T. Calarco, C. P. Koch, W. Köckenberger, R. Kosloff, I. Kuprov, B. Luy, S. Schirmer, T. Schulte-Herbrüggen, D. Sugny, and F. K. Wilhelm, Training Schrödinger's cat: Quantum optimal control, Eur. Phys. J. D **69**, 279 (2015).

[9] T. Caneva, M. Murphy, T. Calarco, R. Fazio, S. Montangero, V. Giovannetti, and G. E. Santoro, Optimal Control at the Quantum Speed Limit, Phys. Rev. Lett. **103**, 240501 (2009).

[10] G. C. Hegerfeldt, Driving at the Quantum Speed Limit: Optimal Control of a Two-Level System, Phys. Rev. Lett. **111**, 260501 (2013).

[11] E. Torrontegui, S. Ibáñez, S. Martínez-Garaot, M. Modugno, A. del Campo, D. Guéry-Odelin, A. Ruschhaupt, X. Chen, and J. G. Muga, in *Advances in Atomic, Molecular, and Optical Physics*, edited by E. Arimondo, P. R. Berman, and C. C. Lin (Academic, New York, 2013) Vol. 62, Chap. 2, pp. 117–169.

[12] A. del Campo, Shortcuts to Adiabaticity by Counterdiabatic Driving, Phys. Rev. Lett. **111**, 100502 (2013).

[13] S. Campbell, G. De Chiara, M. Paternostro, G. M. Palma, and R. Fazio, Shortcut to Adiabaticity in the Lipkin-Meshkov-Glick Model, Phys. Rev. Lett. **114**, 177206 (2015).

[14] V. Mukherjee, S. Montangero, and R. Fazio, Local shortcut to adiabaticity for quantum many-body systems, Phys. Rev. A **93**, 062108 (2016).

[15] S. Campbell and S. Deffner, Trade-off between Speed and Cost in Shortcuts to Adiabaticity, Phys. Rev. Lett. **118**, 100601 (2017).

[16] O. Abah and E. Lutz, Performance of shortcut-to-adiabaticity quantum engines, Phys. Rev. E **98**, 032121 (2018).

[17] K. Funo, J.-N. Zhang, C. Chatou, K. Kim, M. Ueda, and A. del Campo, Universal Work Fluctuations During Shortcuts to Adiabaticity by Counterdiabatic Driving, Phys. Rev. Lett. **118**, 100602 (2017).

[18] Y.-H. Chen, Y. Xia, Q.-C. Wu, B.-H. Huang, and J. Song, Method for constructing shortcuts to adiabaticity by a substitute of counterdiabatic driving terms, Phys. Rev. A **93**, 052109 (2016).

[19] A. C. Santos and M. S. Sarandy, Superadiabatic controlled evolutions and universal quantum computation, Sci. Rep. **5**, 15775 (2015).

[20] I. B. Coulamy, A. C. Santos, I. Hen, and M. S. Sarandy, Energetic cost of superadiabatic quantum computation, Front. ICT **3**, 19 (2016).

[21] A. C. Santos and M. S. Sarandy, Generalized shortcuts to adiabaticity and enhanced robustness against decoherence, J. Phys. A: Math. Theor. **51**, 025301 (2017).

[22] C.-K. Hu, J.-M. Cui, A. C. Santos, Y.-F. Huang, M. S. Sarandy, C.-F. Li, and G.-C. Guo, Experimental implementation of generalized transitionless quantum driving, Opt. Lett. **43**, 3136 (2018).

[23] A. C. Santos, A. Nicotina, A. M. Souza, R. S. Sarthour, I. S. Oliveira, and M. S. Sarandy, Optimizing NMR quantum information processing via generalized transitionless quantum driving, Europhys. Lett. **129**, 30008 (2020).

[24] Y. Susa and H. Nishimori, Variational optimization of the quantum annealing schedule for the Lechner-Hauke-Zoller scheme, Phys. Rev. A **103**, 022619 (2021).

[25] S. Matsuura, S. Buck, V. Senicourt, and A. Zaribafiyan, Variationally scheduled quantum simulation, Phys. Rev. A **103**, 052435 (2021).

[26] A. Bölte and U. W. Thonemann, Optimizing simulated annealing schedules with genetic programming, Eur. J. Oper. Res. **92**, 402 (1996).

[27] J. Roland and N. J. Cerf, Quantum search by local adiabatic evolution, Phys. Rev. A **65**, 042308 (2002).

[28] M. V. Berry, Transitionless quantum driving, J. Phys. A: Math. Theor. **42**, 365303 (2009).

[29] D. Sels and A. Polkovnikov, Minimizing irreversible losses in quantum systems by local counterdiabatic driving, Proc. Natl. Acad. Sci. USA **114**, E3909 (2017).

[30] A. Hartmann and W. Lechner, Rapid counter-diabatic sweeps in lattice gauge adiabatic quantum computing, New J. Phys. **21**, 043025 (2019).

[31] P. W. Claeys, M. Pandey, D. Sels, and A. Polkovnikov, Floquet-Engineering Counterdiabatic Protocols in Quantum Many-Body Systems, Phys. Rev. Lett. **123**, 090602 (2019).

[32] G. Passarelli, V. Cataudella, R. Fazio, and P. Lucignano, Counterdiabatic driving in the quantum annealing of the p-spin model: A variational approach, Phys. Rev. Res. **2**, 013283 (2020).

[33] X. Yao, An empirical study of genetic operators in genetic algorithms, in *Proceedings Euromicro 93 Open System Design: Hardware, Software and Applications*, edited by F. Vajda and B. G. Mortensen, special issue of Microproc. Microprog. **38**, 707 (1993).

[34] L. K. Grover, in *Proceedings of the Twenty-Eighth Annual ACM Symposium on Theory of Computing, Philadelphia, 1996* (ACM, New York, 1996), pp. 212–219.

[35] B. Derrida, Random-energy model: An exactly solvable model of disordered systems, Phys. Rev. B **24**, 2613 (1981).

[36] D. Gross and M. Mezard, The simplest spin glass, Nucl. Phys. B **240**, 431 (1984).

[37] V. Bapst and G. Semerjian, On quantum mean-field models and their quantum annealing, J. Stat. Mech. (2012) P06007.

[38] B. Seoane and H. Nishimori, Many-body transverse interactions in the quantum annealing of the p-spin

ferromagnet, J. Phys. A: Math. Theor. **45**, 435301 (2012).

[39] Y. Seki and H. Nishimori, Quantum annealing with antiferromagnetic fluctuations, Phys. Rev. E **85**, 051112 (2012).

[40] M. Ohkuwa, H. Nishimori, and D. A. Lidar, Reverse annealing for the fully connected p-spin model, Phys. Rev. A **98**, 022314 (2018).

[41] S. Matsuura, H. Nishimori, W. Vinci, T. Albash, and D. A. Lidar, Quantum-annealing correction at finite temperature: Ferromagnetic p-spin models, Phys. Rev. A **95**, 022308 (2017).

[42] Y. Susa, Y. Yamashiro, M. Yamamoto, I. Hen, D. A. Lidar, and H. Nishimori, Quantum annealing of the p-spin model under inhomogeneous transverse field driving, Phys. Rev. A **98**, 042326 (2018).

[43] S. Matsuura, H. Nishimori, W. Vinci, and D. A. Lidar, Nested quantum annealing correction at finite temperature: p-spin models, Phys. Rev. A **99**, 062307 (2019).

[44] G. Passarelli, G. De Filippis, V. Cataudella, and P. Lucignano, Dissipative environment may improve the quantum annealing performances of the ferromagnetic p-spin model, Phys. Rev. A **97**, 022319 (2018).

[45] G. Passarelli, V. Cataudella, and P. Lucignano, Improving quantum annealing of the ferromagnetic p-spin model through pausing, Phys. Rev. B **100**, 024302 (2019).

[46] G. Acampora, V. Cataudella, P. R. Hegde, P. Lucignano, G. Passarelli, and A. Vitiello, An evolutionary strategy for finding effective quantum 2-body Hamiltonians of p-body interacting systems, Quantum Mach. Intell. **1**, 113 (2019).

[47] G. Passarelli, K.-W. Yip, D. A. Lidar, H. Nishimori, and P. Lucignano, Reverse quantum annealing of the p-spin model with relaxation, Phys. Rev. A **101**, 022331 (2020).

[48] G. Acampora, V. Cataudella, P. R. Hegde, P. Lucignano, G. Passarelli, and A. Vitiello, Memetic algorithms for mapping p-body interacting systems in effective quantum 2-body Hamiltonians, Appl. Soft Comput. **110**, 107634 (2021).

[49] K. Deb, A. Pratap, S. Agarwal, and T. Meyarivan, A fast and elitist multiobjective genetic algorithm: NSGA-II, IEEE Trans. Evol. Comput. **6**, 182 (2002).

[50] F.-A. Fortin, F.-M. De Rainville, M.-A. Gardner, M. Parizeau, and C. Gagné, DEAP: Evolutionary algorithms made easy, J. Mach. Learn. Res. **13**, 2171 (2012).

[51] J. Johansson, P. Nation, and F. Nori, QuTiP: An open-source Python framework for the dynamics of open quantum systems, Comput. Phys. Commun. **183**, 1760 (2012).

[52] J. Johansson, P. Nation, and F. Nori, QuTiP 2: A Python framework for the dynamics of open quantum systems, Comput. Phys. Commun. **184**, 1234 (2013).

[53] F. Herrera, M. Lozano, and A. M. Sánchez, A taxonomy for the crossover operator for real-coded genetic algorithms: An experimental study, Int. J. Intell. Syst. **18**, 309 (2003).

[54] D. Chivilikhin, A. Samarin, V. Ulyantsev, I. Iorsh, A. R. Oganov, and O. Kyriienko, MoG-VQE: Multiobjective genetic variational quantum eigensolver, arXiv:2007.04424.

[55] G. E. Crooks, Performance of the quantum approximate optimization algorithm on the maximum cut problem, arXiv:1811.08419.

[56] E. Farhi, J. Goldstone, and S. Gutmann, A quantum approximate optimization algorithm, arXiv:1411.4028.